Research Article

Journal of Geophysical Research: Oceans
DOI 10.1002/2016JC011649

Luigi Cavaleri[1*], Francesco Barbariol[1], Alvise Benetazzo[1], Luciana Bertotti[1], Jean-Raymond Bidlot[2], Peter Janssen[2], Nils Wedi[2]

(1) Institute of Marine Sciences, Venice, Italy

(2) European Centre for Medium-Range Weather Forecasts, Reading, U.K.

The Draupner wave: a fresh look and the emerging view

(*) reference author: luigi.cavaleri@ismar.cnr.it

21 July 2016

Received: Jan 14, 2016; Revised: Jul 22, 2016; Accepted: Jul 25, 2016

Key points

- High resolution and new physics identify key characters of the Draupner storm
- Conditions favourable to freak waves peaked at the time of the Draupner wave
- Definition of the concept of “dynamical swell”

Abstract

Using the new high-resolution operational model of ECMWF, we revisit the storm during which the Draupner freak wave of January 1, 1995 was recorded. The modeling system gives a realistic evolution of the storm highlighting the crucial role played by the southward propagating polar low in creating the extreme wave conditions present at the time the freak wave was recorded. We also discuss the predictability of the meteorological event. The hindcast wave spectra allow a new analysis of the probability of occurrence of the Draupner wave that we analyze not only in time at a specific position, but also in space. This leads us to discuss how exceptional the so-called freak waves really are. For a given sea state, as characterized by the significant wave height, they are namely part of the reality of the ocean, the key point being the probability of encountering them. In this respect, the often considered record at a specific location can be misleading because the probability of detecting a freak wave must be considered both in space and time.

Note:

Index terms

3339 Ocean-atmosphere interactions

3349 Polar meteorology

4255 Numerical modeling

4313 Extreme events

4455 Nonlinear waves

Keywords

Atmosphere-wave-ocean coupling

Hindcast of exceptional events

Forecast of polar lows

The Draupner wave

Statistics of large waves in a storm

1 – The event and the existing related studies

On the 1st of January 1995 the most famous freak wave was recorded by a downwards looking laser beam at the Draupner S platform in the north-central part of the North Sea. Haver (2004), among others, provides a detailed description of the local situation. Several studies, among which the recent one by Magnusson and Donelan (2013), have confirmed the reliability of the measurements and the lack of substantial foam at the crest, i.e. it was a green water wave that passed under the platform. The wave was 25.6 m high, with an 18.5 m crest in a significant wave height sea of almost 12 m. The 20 min long record (once an hour) was taken at 15 UTC.

Besides taking the existence of giant waves out of the limited realm of seamen tales, the record triggered a number of studies and papers aiming at framing the meteorological and wave situation, and providing a physical explanation of the event. The Draupner wave was not the first reported freak wave. Skourup et al (1996) discuss the Gorm wave measured at the Gorm Field on November 17, 1984, in the southern part of the North Sea. Still in the same general area, the North Alwyn wave is cited by Wolfram et al. (2000), and the 2007 Andrea wave by Magnusson and Donelan (2013) who also provide a detailed analysis and intercomparison of the Draupner and Andrea wave characteristics.

Somehow the Draupner wave became the iconic item for the subject and several papers suggested possible explanations for the event, among them Trulsen (2001), Walker et al. (2005), Jensen (2005), and Clauss and Klein (2009). Adcock et al (2011) discuss the various explanations that have been suggested, the most frequent one being the nonlinear focusing of wave energy due to resonant wave-wave interactions (Janssen, 2003; Onorato et al., 2009; Tamura et al., 2009; Waseda et al., 2011). However, the local conditions at Draupner were not really deep water. In 70 m depth with a T_z of 12.5 s, the non-dimensional water depth was $kd = 1.6$ (k the wave number and d the local depth), not far from the 1.36 limit where the Benjamin-Feir index vanishes (Janssen and Onorato, 2007). Besides the directional spreading was not small, but typical of active generation conditions, actually larger as we will see in the next section. None of the other possible mechanisms (linear constructive interference, geometrical focusing, wave-current interaction) provides a plausible explanation.

A key starting point for judging properly the appearance of the giant wave, or at least the related encounter probability (we clarify later our interpretation of this term), is to have a clear view of the meteorological situation that led to the wave conditions at the time and location of the event. Of course the wave triggered a detailed analysis reported by Sunde (1995) and summarized by Haver (2004). The picture often shown reports how a low pressure center was located over Sweden (off the top right in Figure 1 and Figure 2) resulting in a vigorous north-westerly flow. As a consequence, substantial south-east propagating waves covered the whole North Sea. The key extra element however was in the early morning of January 1 when a small polar low (shown in Figures 1 and 2) appeared over the Norwegian Sea (more on this in the next section) moving rapidly south along the main axis of the North Sea. This resulted in an area of increased wind speed to the West of the low that moved quickly southwards, as shown in the two cited figures. The wave conditions followed accordingly, although no detailed overall picture is reported in the literature.

The most recent analysis of the situation we are aware of is by Adcock et al. (2011) who made use of the ERA-Interim reanalysis set-up (Dee et al., 2011) of the European Centre for Medium-Range Weather Forecasts (ECMWF, Reading, U.K.) to revisit the situation. The ERA-Interim resolution is relatively coarse, about 80 km for the meteorological model (even coarser in practice, see Abdalla et al., 2013), but for this specific purpose, the analysis was repeated with the resolution (TL799, about 25 km) as available at the time the study was carried out. The model cycle was 31R2, the one used for ERA-Interim. The analyses are available at six-hour interval (00, 06, 12, 18 UTC) from December 23, 1994 till January 2, 1995. The wave model was WAM (Komen et al., 1994; Janssen, 2008) in its operational coupled version ECWAM available at ECMWF (Janssen, 1991). The coupling, i.e. the two-way interaction between meteorological and wave fields, turns out to be essential in modeling fast growing sea conditions. A relevant result was to highlight the presence of a slight swell (see Figure 2 of Adcock et al., 2011) moving slightly to the left of the main wind sea conditions (throughout the paper we use flow directions).

In this paper, we take a fresh look at the problem by hindcasting the meteorological and wave conditions that characterized the Draupner event using the newly available high resolution model of ECMWF (more in the next section). This has led to a highly detailed description of the overall situation not previously available. Timing of the passage of the polar low turns out to be critical in determining the “when and what” of the local wave conditions. In particular, the moving speed of the low was, according to these new results, one of the relevant factors establishing the local conditions at the time of the event. The meteorological and modeling aspects and the related results are described in Section 2. In Section 3 we then explore the meteorological predictability of the specific Draupner event showing that with the data available in the previous hours, the related meteo-oceanographic conditions could not be foreseen more than about 15 hours in advance. We also include a short analysis of the factors that have led to the present Draupner hindcast, concluding that, given the high quality of the wave model, both improved physics and resolution of the meteorological counterpart are essential in this respect. In Section 4, we use the hindcast results, in particular the directional wave spectra, to focus on the probability aspect of the problem. We perform a thorough analysis of the overall situation, extending the discussion to the general case of freak waves. We approach the problem from two different points of view, considering the encounter probability of supposedly ‘freak waves’ in space (typically one mesh of the grid) and time (the extent of a record, between 20 and 30 min). Still within these limits, a key point is the distinction between occurrence (i.e. happening) and encounter probabilities. We discuss and summarize our findings in the final Section 5.

2 – Meteorological and wave conditions

In this section, we first describe the modeling approach followed to hindcast the storm that generated the Draupner event, then the related main model results are discussed. A third sub-section is devoted to a more detailed analysis of these results, focusing in particular on the wave spectra at the progressive locations of the small, but intense, polar low minimum that characterized the event, and those at the location of the Draupner platform.

2.1 – Modeling

The Integrated Forecasting System (IFS) of ECMWF is a modelling and data assimilation framework for global numerical weather prediction (NWP). The IFS has been used in this study to simulate the atmosphere and the sea surface interaction. The model version CY41R1 has been used with approximately 9 km spatial resolution and 137 hybrid vertical levels between the surface and 0.01hPa, with the lowest model level at approximately 10m above the surface. A novelty of these simulations is the cubic truncation, where $T_{CO}1279$ denotes a triangular spectral truncation with 1279 wavenumbers associated with a cubic reduced Gaussian spectral transform grid on octahedral projection. The latter represents the choice for the now operational (March 8, 2016) high-resolution upgrade of the forecast and analysis system at ECMWF. With a cubic spectral transform grid the IFS orography has more variance and almost no explicit horizontal diffusion and no anti-aliasing filter is applied. Notably, the associated kinetic energy spectra of the cubic grid truncated model have significantly more variance in the mesoscale, see Wedi (2014) and Wedi et al. (2015) for more details. A key point of the new IFS is the full coupling, with the latest parameterizations, between the ocean, wave and atmosphere systems (the ocean coupling was not activated in this study). The latest documentation with detailed descriptions of the dynamical core and the comprehensive physical parameterization package is available from ECMWF (2015).

For waves we have used the ECWAM model, a well established model where all the considered processes are modeled on a physical basis. The model is well documented in the literature (Janssen 2004, Bidlot 2012) and, together with the coupled meteorological and ocean models, provides very good results. Typical bias versus buoy data (not assimilated in the daily procedure) is of the order of a few centimeters for the significant wave height H_s, with scatter index (standard deviation of error divided by the mean measured value) close to 0.10. Typical statistics are available at http://www.ecmwf.int/en/forecasts/charts/medium/comparison-other-operational-centres and at http://www.jcomm.info/index.php?option=com_content&view=article&id=131&Itemid=37 .

The tight coupling in the ECMWF IFS system, especially between the meteorological and wave models, is particularly important in fast growing and steep wind seas (Janssen, 1991, 2004, 2008).

For the present purpose, we have modeled the Draupner storm as a series of 24 hour global forecasts starting from the available analyses out of the cited T799 ERA-Interim (Adcock et al., 2011). The good resolution (25 km) of the previous results allowed a quick development of the field characteristics potentially available from the new 41R1 resolution (9 km). The wave model too runs with high resolution (14 km, 36 directions and 36 frequencies), hence making possible to highlight possible strong local significant wave height H_s gradients.

For the benefit of our present interest, i.e. the Draupner wave, all the results reported below have been obtained starting from the New Year Eve analysis, i.e. January 1, 1995 00 UTC. This was only 15 hours before the event and a discussion on the reasons for this choice is given in Section 3. The output fields (surface wind speed, surface pressure, wave spectrum and derived integral parameters) are available at hourly intervals at all the grid points.

While our focus of interest was on exploring the physics behind the Draupner event, we were also interested in identifying if, as it turned out to be the case, the improvements with respect to the Adcock et al. (2011) study were associated to the improved physics (model cycle 41R1 versus the one used for ERA-Interim (31R2, Dee et al., 2011)) or to the higher (9 versus 25 km) resolution. Therefore an additional experiment was also run, hindcasting the storm with T799 resolution, but with the improved physics. Table 1 summarizes the characteristics of the experiments. This aspect of the results is dealt with in Section 3. All the results shown in Figures 2, 4, and 5 have been obtained with the model cycle 41R1 and high resolution.

2.2 – Modeling results

Figure 2 provides a sequential view of the meteorological maps (surface wind speed (arrows) and surface pressure (isobars at 2 hPa intervals)) at 00, 06, 12 and 15 UTC of January 1 (henceforth we will omit the day when not necessary). The area spans from 52 to 68N and from 4W to 10E. With the forecast starting at midnight, the UTC time in each panel corresponds also to the forecast time range (+ hours). The central low over Sweden is off, to the right of, the map. At +0 h (i.e., 00 UTC, panel a, top-left, analysis) the polar low is clearly visible in the upper right part of the plot as the most enclosed isobar. It is not very deep (at least in this hindcast, see later discussion in Section 3), but it brings with it an energetic increased flux of cold air from the North. At the Draupner platform (the black dot in the central part of each panel) the wind direction is about 135^{o}. In the following hours (panels b and c) the polar low moves rapidly to the South, with increased wind speeds on its front-right area (west in the figure). It reaches the Draupner latitude (panel 2d) at 15 UTC with increased strong wind and a rapid change of its local direction to 180^{o}. In the following hours the low keeps moving South and South-East, reaching at midnight the Dutch coast close to the German border. A good view of the overall situation is given by the satellite picture of 10.41 UTC shown in Figure 3. The polar low, in the North Sea just off the Norwegian coast, is identified by the black circle. Note the northerly flow of cold air towards Scotland identified by the scattered small clouds.

The associated wave fields are shown in Figure 4, panels a to d, for 00, 06, 12, 15 UTC respectively (corresponding to the times in Figure 2). The little white circles identify the sequential position of the wave system associated to the polar low. Following the main field, at 00 the waves at Draupner propagate in South-Easterly direction, remaining as such with little modification until the area of maximum wave heights associated to the polar minimum reaches the Draupner area at 15 UTC. An extensive area of southwards propagating waves follows the polar minimum leading to partly crossed sea conditions at the platform. Here the maximum hindcast significant wave height is close to 11 m, 10.5 m at the time of the freak wave, about 1 m lower than the official measured value. Note the >12 m H_s peak slightly to North-East of the platform. In the following hours the high wave system moves South-South-East, reaching the Dutch coast together with the landing polar low.

So far, we have provided a general picture of the evolution of the pressure low and of the associated wind and wave height fields. We now interpret these results with the aim of identifying the conditions present in the Draupner area at the time the freak wave was measured. This is the subject of the next sub-section.

2.3 – The emerging picture

Summarized in their essential aspect, the conditions at the Draupner were characterized by a well developed wave field with H_s = 6 to 7 m propagating in the 135°-140° direction (panel 4a), progressively growing to H_s = 8 to 9 m at 12 UTC (panel 4c), with a rapid change in propagation direction towards South when the polar minimum, hence the maximum wind speeds, passed at the platform position. The wave directional spreading was certainly not narrow, about 20° in the early part of the day, much more at 15 UTC when the two wave systems, the preexisting one at 135° and the new one at 180° arriving with the low, were superimposed on each other.

A much more interesting detail emerges analyzing the motion of the polar minimum. From the panels of Figure 2, and more so from the corresponding hourly maps (not shown), it is straightforward to estimate the speed with which the low was moving. This turns out to be 55 km h^{-1}, i.e. about 15 m s^{-1}. This is too fast for dynamical generation, i.e. to have a wave system moving with the same speed of the low and continuously receiving energy from it. For such a condition, a wave group speed at 15 m s^{-1}, the wave peak period should be around 19 s, which is much larger than typically found during the Draupner storm. However, granted the average conditions, there was energy in this range or just below it (lower periods). These wave components were moving with the storm, while receiving at the same time energy by nonlinear interactions from the main bulk of the spectrum (and not directly from the wind as their phase speed was higher than the wind velocity, in so doing developing along the course of the low.

The presence of this low-frequency energy is explored in Figure 5 showing the evolution of the wave spectrum in time. The left panels (a1 to a4) show the spectra following the low in its motion, i.e. at the positions in Figure 4 identified with the small white circles. The right panels (b1 to b4) provide the spectra at the Draupner position. The spectra are plotted with constant 20 m^2 s rad^{-1} intervals. This provides a better visualization of their quantitative evolution in time. Also only the (f-θ) area between 0.04 and 0.14 Hz, and 90° and 240° flow directions are shown, where practically most of the wave energy is concentrated.

We begin describing the spectra following the polar low. The initial one at 00 UTC shows only relatively limited wave conditions directed to 200°. At 06 UTC, when the low has entered the main area of the preexisting storm, the conditions are quite different. The locally wind generated spectral components travel to South (180°) with about 12 s period, while longer wave components interact with the preexisting field that still dominates in the lower frequency range where a lobe of the spectrum directed to 120° shows a local swell. At 12 UTC, progressively approaching the freak wave time and location, the peak is now well present at 15 s period directed to 150°. There is always a low frequency (0.055 Hz) lobe to 120°, but a new one, in the same frequency range, but directed to 180°, is emerging. This second peak becomes even more dominant at 15 UTC. We interpret this peak as the "dynamically locked" low frequency part of the spectrum, fed by non-linear interactions from the wind sea part of the spectrum, and moving with, and at the same speed of, the storm. Its frequency, 0.055 Hz and lower, lower than the energetic part of the spectrum, is very close to that of the 19 s waves required to follow the storm in its motion. The sudden appearance of this lobe is even more evident in the right panels of Figure 5, i.e. in the spectra at the platform position. Here the evolution is a combination of the original field at 150° and the incoming one with the low. The key point is that before 15 UTC there is no indication of the 19 s 180° lobe, not even one hour before, at 14 UTC (not shown). It is only at 15 UTC, when, as in panel 2d, the low reaches the Draupner area, that the low frequency wave components following the minimum appear, leading to the spectra shown in panels 5a4 and 5b4. Note the much higher peak value in the former, corresponding to higher H_s area East of the platform as already pointed out. These spectra can be summarized by the following characteristics: a substantial wind-generated system directed at 160°, plus two low frequency lobes, respectively at 120° and 180°, hence at 60° difference, the latter more extended towards the low frequency side.

3 – The predictability of the event

3.1 – The forecast

As stated in Section 2, the starting point for our hindcast has been the TL799 analysis of January 1, 1995 00 UTC (the numerical details are in Table 1). This is only 15 hours before the event of interest, a very short time compared to the predictability regularly available from the present state-of-the-art meteorological models. As an example, the present forecast performance of ECMWF is available at http://www.ecmwf.int/en/forecasts/charts/medium/comparison-other-operational-centres, and also before 2010, when the analyses reported by Adcock et al. (2011) were done, the TL799 then operational model was performing very well. A simple explanation for our approach could be that we were indeed looking for the best picture of the situation of interest. Intuition and practice suggest that, the closer the analysis, the better the forecast. However, in the present case there was another reason. The point is that on the 31st December 00 and 12 UTC analyses (not shown) there was no polar low in the area covered in Figure 2, and also at a longer forecast range. There was a slight reshaping of the isobars of the large low pressure area centered on Sweden, but nothing more than that. The related forecasts, without any further data assimilation, followed accordingly. Figure 6 shows the forecast done with 41R1 (experiment gc8l, details in Table 1) for January 1 15 UTC, i.e. at the time of the freak event, starting from the December 31 00 UTC analysis. This map is to be compared with the one in panel 2d, which started from January 1 00 UTC. The differences are substantial. In Figure 6 the storm, a large feature, is obviously there, driven by the large scale low, but there is no hint of a polar low, hence of all the effects that are associated with its presence. The lesson we derive from these tests is that, independently of the model used for the forecast, there is no way to anticipate the development and evolution of (in this case) the polar low if the relevant information, i.e. the precursors of the phenomenon, are not present in the field we start from, and this in turn depends, not only on the available data, but also on the resolution of model used for the analysis. This is typical for fast evolving systems of limited dimensions, especially in areas that are not sufficiently covered by measurements.

3.2 – Physics and resolution

We have repetitively mentioned how, starting from the TL799 ERA-Interim analysis (details in Table 1), the present high resolution 41R1 model has been capable of following (see Figure 2) the evolution of the polar low with the associated wind and wave interaction processes. These features were not present in the T799 forecast. The two models differ both in physics (cycle 41R1 versus 31R2) and resolution (9 km in our experiments versus the 25 km of TL799 – note that, due to the respective cubic and linear discretization, the effective resolutions are 18 and 100 km respectively). It is natural to ask which one of these aspects was more important in producing such an extreme event as the Draupner wave. This question has been addressed with an experiment, gc9l (see Table 1), where the linear TL799 model was run with the 41R1 physics. The results are given in Figure 7 where we show: a) the 15 h forecast of the original TL799 ERA-Interim model (experiment 1428), b) our more recent forecast from the TL799 run with the present physics (gc9l). These results are to be compared with panel 2d, i.e. the one with the latest model physics and resolution. From the two panels in Figure 7 we see that the new physics in itself fails to maintain in time, starting from the 00 UTC analysis, the identity of the polar low that, as a limited extension, has now become part of the large Swedish low. There is a very mild increase of the spatial gradients in the area of the Draupner in panel 7b (new physics) with respect to 7a, but it is evident that the major improvements leading to the results plotted in Figure 2 are due to the increased resolution. This is what has allowed the identification of what we consider a key element in determining the conditions for the Draupner freak wave.

4 – Analysis of the event

In this section, we discuss the Draupner wave in the light of the achieved model results, resorting to some recent findings concerning the distributions of extreme wave and crest heights. For this purpose it is natural to use the best results, i.e. the ones out of the run with the new physics and resolution (experiment gc8m in Table 1), already reported in Figures 2, 4 and 5. These wave spectra resulting from the described new atmospheric and wave modeling are regarded as the basis for our analysis of extremes using two different approaches. The first one is a novel theoretical model by Janssen (2015) who focuses on the tail of the non-linear distribution of the envelope wave height. The second one stems from the theoretical development of space-time extreme wave statistics due to Fedele (2012), and applied by Benetazzo et al. (2015) in a non-linear context. We first use both theories to derive the Draupner wave probability of occurrence, and then we discuss what we consider the correct view of any similar event. A more thorough analysis of the effects on extreme waves of non-linearity and space-time evolution will be given in a parallel forthcoming paper.

4.1 – The probability of the Draupner wave

What made the Draupner wave famous was 1) being the first documented major wave height, 2) the large $H_{max}/H_s = 2.4$ and $C_{max}/H_s = 1.55$ values, 3) the apparently odd asymmetry, 18.5 m crest height out of 25.6 m wave height. There is no agreed definition of freak wave, the common threshold value of H_{max}/H_s varying between 2 and 2.2. This is of course nonessential, because, for a given sea state, what is important, particularly for the extreme value analysis, is the wave height parent distribution (see Goda, 2000 and Waseda, 2011). However, the word is now part of the common terminology, easily leading to a feeling of having too frequently exceptional waves. For instance the former value, 2, is in our opinion too low because even in the standard Rayleigh distribution it is expected for one wave out of about 3,000. 3,000 waves correspond to less than ten hours at any given position in a severe storm.

Our first analysis of the probability of the specific event is based on the work of Janssen (2014, 2015) who, starting from the method suggested by Goda (2000), based his approach on the statistics of the envelope wave heights. Rather than on the single wave heights, Janssen assumed as independent events the sequential wave groups in a record, in turn depending on the relative width of the spectrum and its mean frequency. Extensive numerical tests provided results in good agreement with theory (Janssen, 2015), supporting this approach as suitable for estimating the probability of extreme events. The extension of this approach into the weakly nonlinear regime shows that, for what wave height is concerned, the non-linearity of the system has limited effects for modest values of H_{max}/H_s in the range of 2.0 to 2.5. However, things change substantially in the extreme value range. In fact, there is evidence (e.g., Janssen, 2014) that the pdf of envelope wave height of very extreme sea states has an exponential tail, which leads to much larger probability of occurrence for extreme events. In this respect, Janssen (2015) succeeded in estimating the nonlinear probabilities of an event up to h values (the envelope height divided by the significant wave height) greater than 3 (see Figure 8). While taking non-linearity into account substantially enhances the probability of freak events (whichever their definition) for $h > 2.0$, further enhancement is obtained, for $h > 2.7$. We have exploited these results estimating the probability of the specific Draupner event using the model estimated wave spectrum at 15 UTC, analyzing the event not only in time at a specific position, but also in the 2-D space at a specific time. For the latter we have used the 14x14 km^2 area corresponding to the wave model grid mesh. This "spatial" probability of exceedance jumps up to 24%, compared to 1.0% of the linear method.

We have also used a different approach based on the estimation of the maximal crest height probability over a bounded space-time region, following the Euler Characteristics (EC) approach (Adler, 2000). In this case, wave crests are considered as maximal sea surface elevations of specific wave groups evolving over the 2-D horizontal space as well as in time (Fedele, 2012). The EC approach allows a definition of the exceedance probability of the space-time extreme elevations, from which one can derive the expected value of the maximal crest height. In this respect, Fedele (2012, 2015) and Benetazzo et al. (2015) provide the derivation and relevant nonlinear formulas. Validity of such an approach has been discussed in the study by Barbariol et al (2015), using numerical simulations, and by Fedele et al. (2013), and Benetazzo et al. (2015) who, using two stereoscopic video cameras from the ISMAR oceanographic tower (Cavaleri, 2000), obtained four-dimensional (3D in space + time) detailed and accurate measurements of an extensive sea surface area during stormy conditions. The analysis of stereo data confirmed the contribution of second order nonlinearities (Tayfun, 1980, Fedele and Tayfun, 2009) to the space-time extreme values of the crest height. The directional wave spectrum (panel b4 of Figure 5) has been used to compute, via EC approach, the nonlinear probability that the maximal crest height exceeds, at a given instant, the Draupner value ($C_{max} = 1.55\ H_s$) over a spatial region with area of 14x14 km2. Indeed, using the spectral moments, an estimate of the average number of 2-D waves in the spatial domain is derived. The nonlinear contribution is related to the wave steepness that has been obtained following Fedele and Tayfun (2009) (as directly verified, also using the definitions provided by Janssen (2009) the result did not change significantly). Then, given the number of spatial 2-D waves and the steepness, the probability that Cmax exceeds $1.55H_s$ has been found equal to 22% at 14 UTC and 17 % at 15 UTC, close to the estimate obtained using the Janssen (2015) approach.

As a further and final step, we have evaluated the area of the sea surface region required to have as maximum expected space-time extreme the crest height measured at Draupner over the 20-minutes record. The extent turns out to be 800x800 m^2.

The different spatial extents and probabilities derived with the different approaches are further clarified in the next sub-section dealing with the concept of encounter probability.

4.2 – The encounter probability

In dealing with events such as the Draupner wave, we have a tendency to marvel at the supposedly exceptional phenomenon and to wonder what is the probability that such an event occurs. Then the hunt starts for the "culprit", i.e. the process that led to the generation of the event. There is a bias in all this. Richard Feynman, the Nobel laurate, used to enter his class saying "do you know what happened to me? Just before entering the institute I saw a car with the plate YX948BG! Can you imagine? Of all the possible plates just that one! What was the probability?". Of course the fact would have been exceptional if he had mentioned that plate number the day before. It is the same with freak events (as with any other exceptional event). Out of the thousands of records daily collected we focus, a posteriori, just on the one, and once in a while, where the freak event materialized. It is like approaching a lottery winner and marveling at the probability that he would be the one. The truth we suggest is that there is nothing exceptional about these events. Granted some solid physics beyond the linear theory, these events do happen, sometime, somewhere, everywhere. It is just a matter, to notice them, of being at the right (or wrong) time at the right spot. Casas-Prat and Holthuijsen (2010) had hinted to this showing how the statistics of very long time series from a set of Mediterranean Spanish buoys fits well the Rayleigh distribution. However, these results suggest that possibly they missed the deviation from this distribution for the largest values, possibly either because of the relatively low number of samples in the highest range and/or because of the tendency of the buoys to slide aside the highest crests. Another example of the correct approach is given by Waseda et al. (2011) analyzing 2723 20-min stormy records in the North Sea, comparing the number of times a freak wave (i.e. twice the significant wave height) appeared with the expected number according to the theoretical probability.

Following Petrauskas and Aagard (1971), we propose that, instead of "happening or occurrence probability", the expression "encounter probability" is used. In so doing we imply that the low probability must not refer to the phenomenon itself, relatively ubiquitous in the oceans, but rather to the chance of being where and when it happens. Of course, as shown by Fedele (2012), the encounter probability depends on the time and space extend we consider. Indeed the concept of "encounter probability" is often used in climatic terms or, in other words, to define for instance the design or 100 year wave for a structure. The concept is the same, but we use it on the time scale of a record, typically between 20 and 30 min, but with a broader view in space. This has practical implications. For instance it follows that, because of the different spatial dimension, such a probability is higher for a ship than for a buoy. Fedele (2012) made clear this point about the encounter probability with a freak wave. Indeed taking the buoy point of view would imply to discuss the probability that a freak wave hits a precise predefined position of a ship or a rig. So, the larger the structure, the larger the encounter probability. In a way, to know that in, e.g., the square mile where our boat is there is a 15% probability, in the next 20 minutes, of a freak wave may put the problem in a different perspective.

5 – Discussion and summary

A freak wave is by definition a rare event. Therefore, also devising a mechanism or identifying the conditions under which the encounter probability is substantially enhanced, still we are at the mercy of the sea for coming across this rare beast where records by instruments are available. Hence a proof can only be provided, statistically at least, with long term analysis of recorded data, better if also in space, and not only in time. Casas-Prat and Holthuijsen (2010) and Waseda et al. (2011) followed this approach analyzing respectively a very large number of records off the Spanish Mediterranean coast and in the North Sea. Both these studies failed to find a higher probability of normalized large wave heights with respect to the Rayleigh distribution. At the same time a large number of studies support better fits to the overall wave height (and crest) distribution with second or higher order theories, as documented by Tayfun (1980), Forristall (2006), Tayfun and Fedele (2007). One of the frequently reported characteristics of the freak waves, as in the case of Draupner, is to be characterized by a single very high crest, while the previous and following waves do not show particular characteristics. Benetazzo et al. (2015) stressed that many of the assumed freak events can be simply the passage of a wave at the highest point of the envelope of a particularly large space-time group. The key point would be to look also in space, not only in time. This is why we consider the expression "encounter probability" more representative of true ocean events than the more commonly used "happening or occurrence probability", the latter conveying too much the idea of a physically rare event. On the contrary, supported by theory and 3+1 D (three-dimensional in space plus time) experimental data, we claim that these, e.g., particularly high crests are part of everyday life, the crucial point from the user perspective being the probability of encountering them. In turn this depends on the span of space and time considered.

Our hindcast of the Draupner storm provides significant wave heights somehow underestimated (-1 m) with respect to the measured value (close to 12 m). This latter figure may be somewhat biased high by the presence of the freak wave. At the same time an underestimate of H_s may have derived from an underestimate of the wind speed by the model, e.g. with an insufficient deepening of the polar low, a non-satisfactory physics of the wave model in particularly difficult (e.g., crossed sea) conditions, or simply by a small shift, in space and/or time, of the position of the low when passing close to the platform. In this respect, we have noted in Figure 4d the higher wave conditions (H_s > 12 m) to the right (eastwards) of the tower position, seen also in the spectra of panels a4 vs b4 in Figure 5. This is not the main point, here at least. The high resolution hindcast has been able to provide results, as the 2D spectra, from which we have locally deduced a substantial overall encounter probability of very large waves. We point how, rescaling the modeled spectra according to the measured significant wave height, for instance assuming the spectrum in panel 5a4 as at the Draupner position (an action we have purposely not done for the implied approximation), would substantially reduce the encounter space and time extents we have reported as derived from the statistical approaches described in Section 4, bringing the Draupner wave within the range of an almost expected event.

Another product of the high resolution hindcast is the presence in the 2D spectrum of a low frequency swell, swell because with a phase speed faster than wind. However this swell was moving with the polar low system, in so doing receiving energy by nonlinear interactions from the system active wind waves. Hence we propose the expression "dynamical swell" to convey the idea of a non-passive swell advection. We suggest that a similar situation may arise whenever a storm propagates in the direction of the main waves it generates with a speed similar to the group speed of the low frequency part of the spectrum off the main peak.

A point we have not discussed because it is not the dominant one, but potentially relevant for the correct figures, is the simultaneous arrival of the two cross wave systems, particularly in the low frequency range, one, directed to South-East, associated to the pre-existing large pressure low, the second, pointing South, coming along with the polar low. Onorato et al. (2006) had shown how this situation can lead to an enhanced probability of freak waves, and this was interpreted by Cavaleri et al. (2012) as the possible reason for the Louis Majesty cruise accident (two persons killed on board). In the case of the Draupner, the dynamical swell has been estimated as only a fraction of the overall energy. Therefore we do not believe it was at the base of the measured freak wave. However, the possibility exists of having, partially at least, contributed to enhance the encounter probability. Also this result suggests that freak waves may arise due to different processes, and not only, or mainly, from the modulational instability classically dealt with by Onorato (2006) and nicely discussed for practical applications by, among others, Waseda et al. (2014).

This stresses that, while, supported also by the existing theory, we believe that these so-called freak events are indeed, in space and time, more common than previously supposed, some other aspects of theory are still to be explored. The sea, and waves in particular, have a basically nonlinear behavior. Our convenient spectral approach for wind waves, derived from the 1952 paper by Pierson and Marks (1952), omitted the nonlinear part of the system, and with what are indeed amazingly good results. However, it was only ten years later that Hasselmann (1962) pointed out one of the implications of non-linearity in the system. Much has been done in this direction, but we believe much is still to be uncovered out of the veil that still hides it. If in the long term this is the best approach is something that would deserve a thorough discussion.

On the meteorological and oceanographic side, we have seen that the physics of the coupled ECMWF modeling system and its resolution are part of where substantial improvements are still possible, and certainly necessary for extreme, or also simply intense, events. In the case of the polar low, we have seen how the spatial resolution is essential in properly simulating situations locally dominated by a small, but intense, event. The parallel with typhoons and hurricanes, or explosive cyclogeneses, is obvious. We have also seen how with a sufficiently detailed physics we may be able to keep the identity of the small scale system during the course of time. Again, as in the case of wind waves non-linearity, we believe further advancements are required.

It was remarkable that the polar low was noticeable in the analysis map only when already on its way to South. Indeed its whole trajectory from the far North (about 66^o N), where it was identified, till the Dutch coast took less than 24 hours. No hint of its existence, hence no possible prediction, was there before January 1, 00 UTC. This hints to a lack of locally measured data, nowadays possibly partly corrected because of the interest in the Arctic. However the general question of poorly documented areas remains.

We can summarize our findings in the following compact statements:

1 –the "buoy" point of view of the probability of a freak wave may be misleading. During a storm the problem must be considered in space and time. Then we argue that these supposedly exceptional events are relatively common, and part of the reality, especially when the nonlinear aspects of wind waves are considered,

2 – it follows that, with respect to the "buoy" single point of view, the short-term "encounter probability" increases with the spatial dimension of, e.g., the structure we are considering. This is why we favor and propose the expression "encounter" rather than "happening or occurring" probability,

3 – under this perspective the Draupner eventloses much of its glamor of rare event. It is just a matter of probability of coming across, a probability to be considered both in space and time,

4 – however, in the case of the Draupner the wave conditions, both as height and spectral shape, were very favorable to the encounter with a particularly high wave and crest. This may have been enhanced by the presence of two large crossing wave systems with also two substantial lobes of energy in the low frequency range,

5 – in the latter respect we have introduced the concept of "dynamical swell" to identify that part of the wave spectrum moving with the storm without receiving energy from the wind because of its higher phase speed, but fed via nonlinear interactions from the wind active part of the spectrum, This condition may be more common than expected, particularly with fast moving storms.

6 – the combined physics and resolution of the meteorological and coupled models are capable to identify and follow small scale events, more in general those with strong spatial and temporal gradients. However, the uninterrupted progress, as also the model results, suggest that further improvements are possible and often necessary,

7 – in the case of the polar low we have been able to follow its existence and unity as a system all along its track. However, the model results suggest, among other possibilities, that higher than modeled wind speeds were present, i.e. that a higher resolution would be required,

8 – the polar low, and its precursory situation, were not identified till when well formed off the coast of Norway. Twenty years have passed of course, but this points to the need of enough measured data wherever small, but intense, systems characterized by a rapid development are possible.

Acknowledgements

The data used for the present analysis are available at the European Centre for Medium-Range Weather Forecasts (Reading, U.K.). Due to the rules of the Centre they can be asked to Jean-Raymond Bidlot (co-author, jean.bidlot@ecmwf.int).

Francesco Fedele suggested to repeat the Draupner hindcast with high resolution. The modeling work was carried out during a one month staying of Luigi Cavaleri and Luciana Bertotti at the European Centre for Medium-Range Weather Forecasts. Their hospitality, use of facilities and data, and help, in particular by Saleh Abdalla and Dominique Lucas, are gratefully acknowledged. During this staying Luciana Bertotti was supported by the 2015 Short Term Mobility Program of the Italian National Research Council. The satellite picture of Figure 3 had been recorded by the Dundee Satellite Receiving Station and it has been kindly provided by Linus Magnusson and Tim Hewson. Alvise Benetazzo and Francesco Barbariol thank the support from the Flagship Project RITMARE— The Italian Research for the Sea—coordinated by the Italian National Research Council and funded by the Italian Ministry of Education, University and Research within the National Research Program 2011–15.

The suggestions by two Reviewers, Robert Jensen and another anonymous one, are acknowledged for their competence and for having led to an improved and clearer version of the paper.

References

Abdalla,S., L.Isaksen, P.A.E.M.Janssen, and N.Wedi,2013. Effective spectral resolution of ECMWF's atmospheric forecast models, ECMWF Newsletter Nr. 137, p19-22.

Adler, R.J., 2000. On excursion sets, tube formulas and maxima of random fields. *Ann. Appl. Probab.*, **10**, 1–74.

Adcock, T.A.A., P.H.Taylor, S.Yan, Q.W.Ma, and P.A.E.M.Janssen, 2011. Did the Draupner wave occur in a crossing sea?, *Proc. of the Royal Soc.A*, June 15, 18p.

Barbariol F., A. Benetazzo, S. Carniel, M. Sclavo, 2015. Space–Time Wave Extremes: The Role of Metocean Forcings. *J. Phys. Oceanogr.*, **45**, 1897–1916. DOI.10.1175/JPO-D-14-0232.1.

Benetazzo, A., F.Barbariol, F.Bergamasco, A.Torsello, S.Carniel, and M.Sclavo, 2015. Observation of extreme sea waves in a space-time ensemble. *J. Phys. Oceanogr.*, **45**, 2261–2275., DOI.10.1175/JPO-D-15-0017.1.

Bidlot J.-R., 2012. Present status of wave forecasting at ECMWF. Proceeding from the ECMWF Workshop on Ocean Waves, 25-27 June 2012.

Casas-Prat, and L.H.Holthuijsen, 2010. Short-term statistics on waves observed in deep water, *Journal of Geophysical Research*, Vol.115, C09024, 20p, doi:10.1029/2009JC005742,2010.

Cavaleri, L., L.Bertotti, L.Torrisi. E.Bitner-Gregersen, M.Serio, and M.Onorato, 2012. Rogue waves in crossing seas: The Louis Majesty accident, *Journal of Geophysical Research*, VOL. 117, C00J10, 8p., doi:10.1029/2012JC007923

Clauss, G.F., and M.Klein, 2009. The new year wave: spatial evolution of an extreme sea state, *J. Offshore Mech. Arctic Eng*., **131**, 041001, (doi:10.1115/1.3160533).

Dee, D.P., S.M.Uppala, A.J.Simmons, P.Berrisford, P.Poli, S.Kobayashi, U.Andrae, M.A.Balmaseda, G.Balsamo, P.Bauer, P.Bechtold, A.C.M.Beljaars, L.van de Berg, J.-R.Bidlot, N.Bormann, C.Delsol, R.Dragani, M.Fuentes, A.J.Geer, L.Haimberger, S.B.Healy, H.Hersbach, E. V.Hólm, L.Isaksen, P.Kållberg, M.Köhler, M.Matricardi, A.P.McNally, B. M.Monge-Sanz, J.-J.Morcrette, B.-K.Park, C.Peubey, P.de Rosnay, C.Tavolato, J.-N.Thépaut, and F.Vitart**,** 2011. The ERA-Interim reanalysis: configuration and performance of the data assimilation system, *Quart. J. Royal Meteor. Soc*, **157**, Issue 656, 553-597, April 2011, Part A.

ECMWF, 2015. IFS documentation, https://software.ecmwf.int/wiki/display/IFS/Official+IFS+Documentation

Fedele, F., Tayfun, M.A., 2009. On nonlinear wave groups and crest statistics. J. Fluid Mech. 620, 221–239.

Fedele, F., 2012. Space–Time Extremes in Short-Crested Storm Seas. J. Phys. Oceanogr. 42, 1601–1615.

Fedele, F., A.Benetazzo, G.Gallego, P.-C.Shih, A.Yezzi, F.Barbariol, and F.Ardhuin, 2013: Space– time measurements of oceanic sea states. *Ocean Model.*, **70**, 103–115, doi:10.1016/j.ocemod.2013.01.001.

Forristall, G. Z., 2006: Maximum Wave Heights Over An Area And The Air Gap Problem. *Proceedings of OMAE06, 25th International Conference on Offshore Mechanics and Arctic Engineering*, June 4-9, Hamburg, Germany, 1–5.

Goda, Y., 2000. Random seas and Design of Maritime Structures. 2nd ed. World Scientific, 464 pp.

Hasselmann, K., 1962: On the non-linear energy transfer in a gravity-wave spectrum, part 1: general theory., *J. Fluid Mech.* 12, 481-500.

Haver, S., 2004. A possible freak wave event measured at the Draupner jacket January 1 1995. In *Rogue Waves Workshop, Brest*. (www.ifremer.fr/web-com/stw2004/rw/fullpapers/walk_on_Haver.pdf).

Janssen, P.A.E.M., 1991. Quasi-linear theory of wind wave generation applied to wave forecasting, *J. Phys. Oceanogr.*, **21**, 1631-1642, doi: http://dx.doi.org/10.1175/1520-0485(1991)021<1631:QLTOWW>2.0.CO;2

Janssen, P.A.E.M., 2003. Nonlinear four-wave interactions and freak waves, *J. Phys. Oceanogr*., **33**, 863-884 (doi:10.1175/1520-0485(2003)33<863:NFIAFW>2.0.CO:2).

Janssen, P. 2004. *The Interaction of Ocean Waves and Wind*. Cambridge University Press, 308+viii pp.

Janssen, P.A.E.M., 2008, Progress in ocean wave forecasting, *J. Comput. Phys.*, **227**, 3572-3594.

Janssen, P.A.E.M., 2014. On a random time series analysis valid for arbitrary spectral shape, J. Fluid Mech. 759, 236-256.

Janssen, P.A.E.M., 2015. How rare is the Draupner wave event?, ECMWF, Technical Memorandum 775, 26pp.

Janssen, P.A.E.M., and M.Onorato, 2007. The intermediate water depth limit of the Zakharov equation and consequences for wave prediction, *J. Phys. Oceanogr*., **37**, 2389/2400 (doi:10.1175/JPO3128.1).

Jensen, J.J., 2005. Conditional second-order short-crested water waves applied to extreme waves episodes, *J. FluidMech*., **545**, 29-40 (doi:10.1017/S0022112005006841).

Komen, G.J., L.Cavaleri, M.Donelan, K.Hasselmann, S.Hasselmann and P.A.E.M.Janssen, (1994), *Dynamics and Modeling of Ocean Waves*, Cambridge University Press, 532p.

Magnusson, A.K., and M.A.Donelan, 2013. J.*Offsh. Mech. and Arctic Eng.*, **135**, 031 108, 10p.

Onorato, M., A.R.Osborne, and M.Serio, 2006. Modulational instability in crossing sea states: a possible mechanism for the formation of freak waves, *Phys. Rev. Lett*., **96**, 014503.

Onorato, M., L.Cavaleri, S.Fouques, O.Gramstad, P.A.E.M.Janssen, J.Monabliu, A.R.Osborne, C.Pakodzi, M.Serio, C.Stansberg, A.Toffoli, and K.Trulsen, 2009. Statistical properties of directional ocean waves: the role of the modulational instability in the formation of extreme events, *Phys. Rev. Lett*., **102**, 114502 (doi:10.1103/PhysRevLett.102.114502).

Petrauskas, C., and P.M.Aagard, 1971. Extrapolation of historical storm data for estimating design-wave heights, *J. of Petroleum Engineers*, March 10971, 23-27, Trans., AIME, 251.

Pierson, W.J., Jr and W.Marks, 1952. The power spectrum analysis of ocean-wave records, *Trans. Amer. Geophys. Union*, 33, 834-844.

Skourup, J.K., K.Andreassen, and N.H.O.Hansen, 1996. Non-Gaussian extreme waves in the central North Sea, *Proceedings of the 1996 OMAE*, **Vol.1**, Part A, ASME, New York.

Sunde, Alf, 1995. 'Kjempebølger i Nordsjøen' (Big waves in the North Sea). 17-23. Nr 2/1995, Årgang 19. Universitetsforlaget. ISSN 0803-3293 (in Norwegian)

Tamura, H., T.Waseda, and Y.Miyazawa, 2009. Freakish sea state and swell-windsea coupling: Numerical study of the *Suwa-Maru* incident, *Geoph. Res. Lett*., **36**, L01607, doi:10.1029/2008GL036280.

Tayfun, M.A., 1980. Narrow-band nonlinear sea waves. J. Geophys. Res. 85, 1548–1552.

Tayfun, M. A., and F.Fedele, 2007: Wave-height distributions and nonlinear effects. *Ocean Eng.*, **34**, 1631–1649, doi:10.1016/j.oceaneng.2006.11.006.

Trulsen, K., 2001. Simulating the spatial evolution of a measured time series of a freak wave. In *Proc.of Rogue Waves 2000*, 29-30 November 2000 (eds M.Olagnon and M.Athanassoulis), 265-273.

Walker, D.A.G., P.H.Taylor, and R.Eatock Taylor, 2005. The shape of large surface waves on the open sea and the Draupner New Year wave, *Appl. Ocean Res.*, **26**, 73-83 (doi:10.1016/j.apor.2005.02.001).

Waseda, T., M.Hallerstig, K.Ozaki, and H.Tomita, 2011. Enhanced freak wave occurrence with narrow directional spectrum in the North Sea, *Geoph. Res. Lett.*, **38**, L13605, doi:10.1029/2011GL047779.

Waseda, T., K.In, K.Kiyomatsu, H.Tamura, Y.Miyazawa, and K.Iyama, 2014. Predicting freakish sea state with an operational third-generation wave model, *Nat. Hazards Earth Syst. Sci.*, **14**, 945-957.

Wedi, N.P., 2014. Increasing horizontal resolution in NWP and climate simulations: illusion or panacea?, Phil.Trans.R.Met.Soc., A 372, 20130289.

Wedi, N.P., P.Bauer, W.Deconinck, M.Diamantakis, M.Hamrud, C.Kubnlein, S.Malardel, K.Mogensen, G. Mozdzynski, and P.Smolarkiewicz, 2015. The modelling infrastructure of the integrated forecast system: Rcent advances and future challenges. Tech.Rep. 760, ECMWF, Reading, U.K..

Wolfram. J., B.Linfoot, and P.Stansell, 2000. Long and short-term extremes statistics in the North Sea: 1994-1998, in Rogue Waves 2000, 363-372.

Figure captions

Figure 1 – The progressive motion of the area of strong winds following the polar low in the North Sea according to the analysis by Sunde (1995) as reported by Haver (2004). The date is 1st of January, 1995.

Figure 2 – Wind speed (arrows) and surface pressure (isobars) distribution in the North and Norwegian seas on 1st of January, 1995. Isobars at 0.5 HPa interval. The dot shows the position of the Draupner platform. The position of the polar low is given by the smallest closed isobar in the grey area. Panels a to d at 00, 06, 12, 15 UTC respectively. See Figure 4 for the corresponding wave fields.

Figure 3 – Satellite picture from AVHRR Channel 4 of the NOAA 9 polar orbiting satellite. The circle shows the position of the polar minimum during its fast South going motion. Time is 10.41 UTC January 1, 1995.

Figure 4 – Significant wave height (m) distribution in the North and Norwegian seas on 1st of January, 1995. Isolines at 0.5 m interval. The black dot shows the position of the Draupner platform. The white circles show the positions of the spectra in panels a. of Figure 5. Panels a to d at 00, 06, 12, 15 UTC respectively. See Figure 2 for the corresponding wind and surface pressure fields.

Figure 5 – Two dimensional (f-θ) wave spectra at (1 to 4) 00, 06, 12, 15 UTC respectively. Panels a. are at a position (small white circles in Figure 4) slightly to the West of the polar low (see its positions in Figure 2). Panels b. are at the Draupner position (black dot in Figure 4). Energy density isolines at 20 m^2 s rad^{-1} interval. Only the area between 0.04 and 0.14 Hz, and 90° and 140° flow directions, where energy is concentrated, is shown. Positions are as latitude North and longitude East.

Figure 6 - Wind speed (arrows) and surface pressure (isobars) distribution in the North and Norwegian seas starting from the December 31 00 UTC analysis at +39 h forecast for 1st of January, 1995 15 UTC. Isobars at 0.5 hPa interval. The dot shows the position of the Draupner platform. Experiment gc8l (see Table 1).

Figure 7 - Wind speed (arrows) and surface pressure (isobars) distribution in the North and Norwegian seas on 1st of January, 1995 15 UTC. 15 h forecasts from the 00 UTC analysis. Isobars at 0.5 hPa interval. The dot shows the position of the Draupner platform. Panel a according to the 1428 experiment. Panel b according to the gc9l experiment. See Table 1 for their specifications.

Figure 8 - Envelope wave height probability distribution function (normalized with respect to H_s) of the Draupner wave in an area 14x14 km^2, starting from the wave conditions represented by the spectra in panels a4 and b4 of Figure 5. Linear, nonlinear, and nonlinear with exponential tail distributions are considered..

Table captions

Table 1 – Characteristics of the different experiments whose results are discussed in this paper. The 1428 experiment is the one by Adcock et al. (2011).

Table 1 – Characteristics of the different experiments whose results are discussed in this paper. The 1428 experiment is the one by Adcock et al. (2011).

experiment	model cycle	spectral resolution	spatial resolution (km)	initial conditions
gc8m	41R1	T1279L137	9	00 01Jan1995
gc8l	41R1	T1279L137	9	00 31Dec1994
gc9l	41R1	TL799L137	25	00 01Jan1995
1428	ERA-Interim (31R2)	TL799L60	25	00 01Jan1995

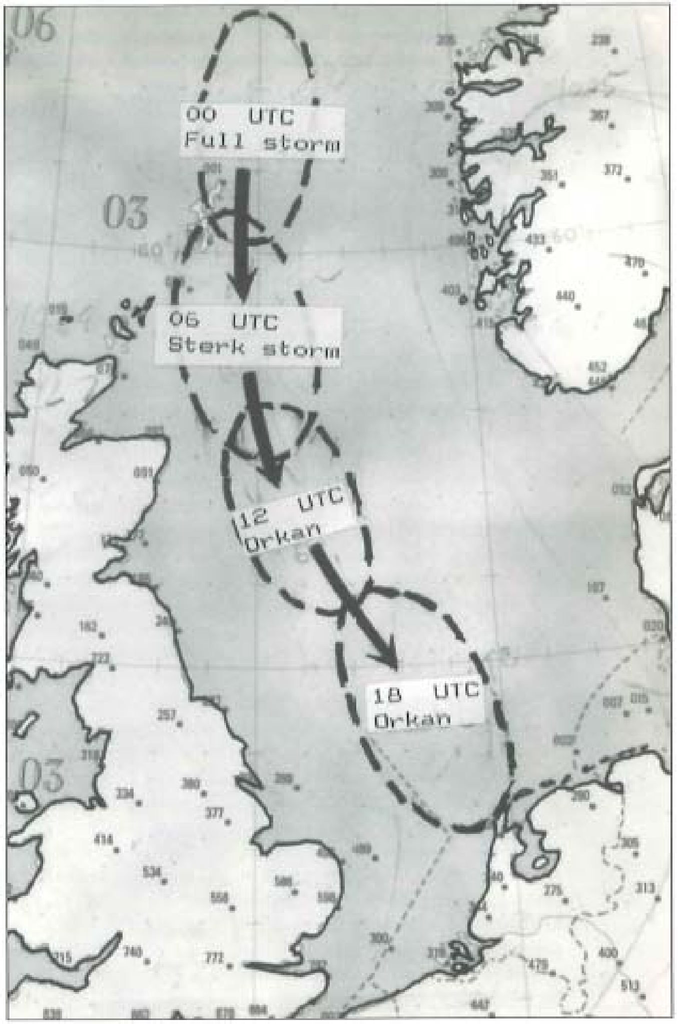

Figure 1 – The progressive motion of the area of strong winds following the polar low in the North Sea according to the analysis by Sunde (1995) as reported by Haver (2004). The date is 1st of January, 1995.

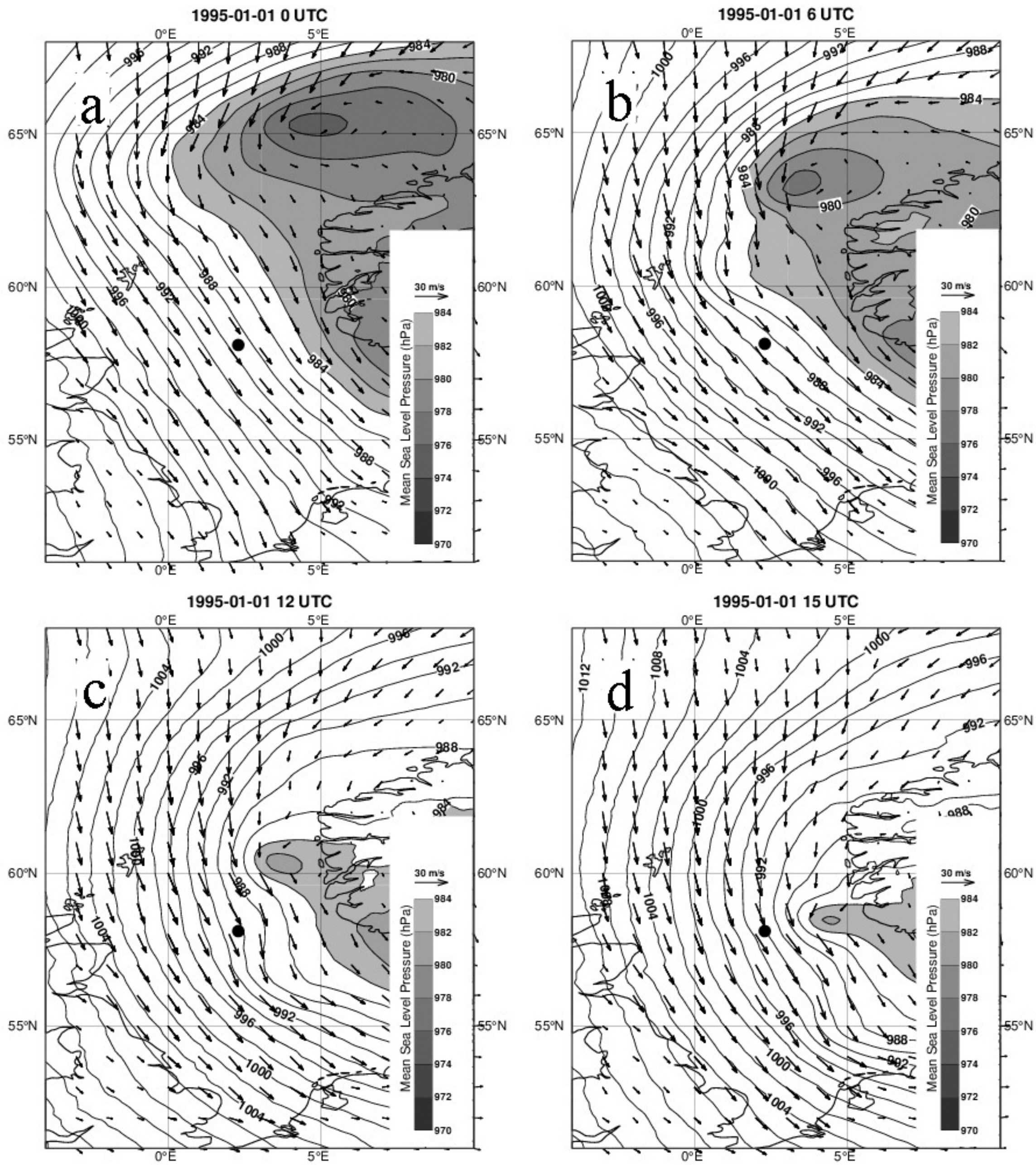

Figure 2 – Wind speed (arrows) and surface pressure (isobars) distribution in the North and Norwegian seas on 1st of January, 1995. Isobars at 0.5 HPa interval. The dot shows the position of the Draupner platform. The position of the polar low is given by the smallest closed isobar in the grey area. Panels a to d at 00, 06, 12, 15 UTC respectively. See Figure 4 for the corresponding wave fields.

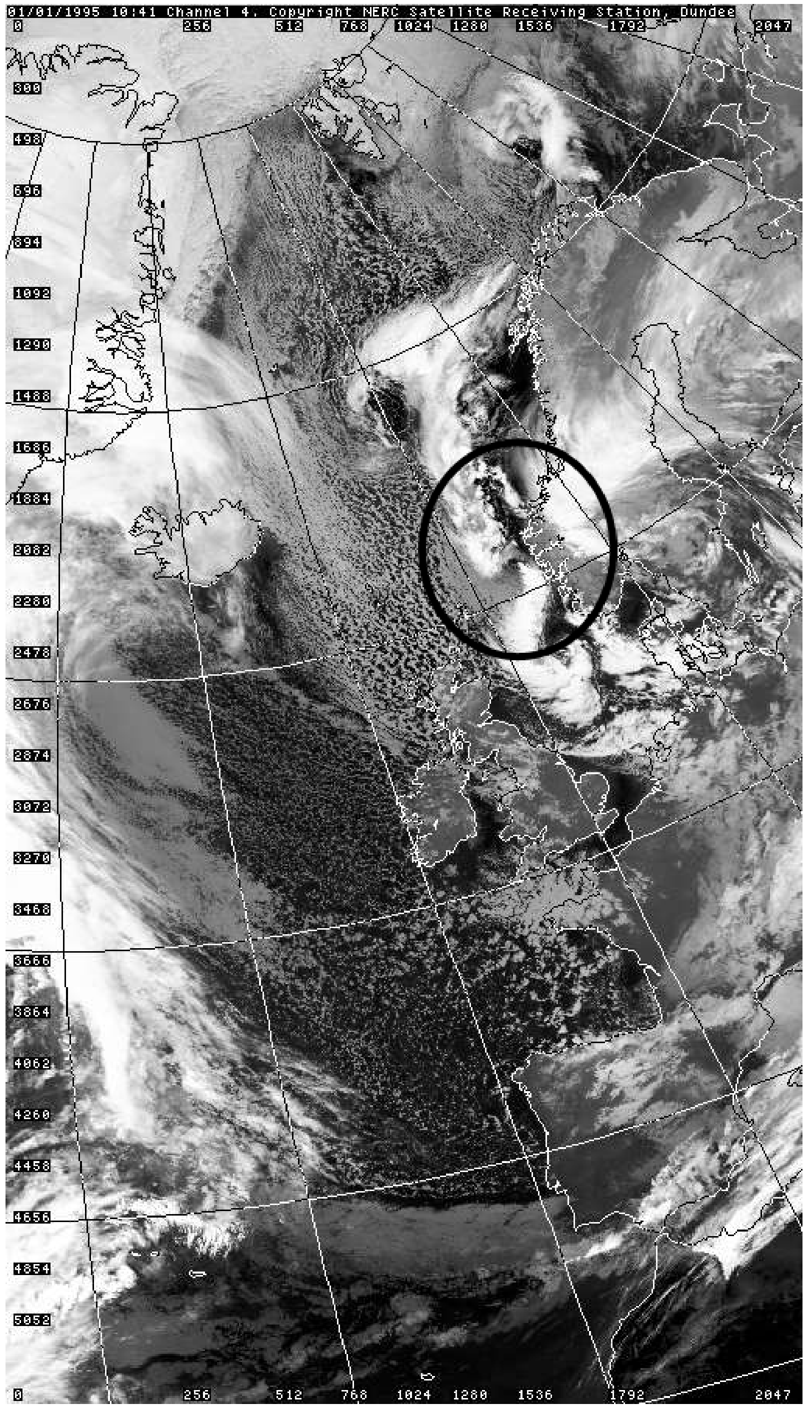

Figure 3 – Satellite picture from AVHRR Channel 4 of the NOAA 9 polar orbiting satellite. The circle shows the position of the polar minimum during its fast South going motion. Time is 10.41 UTC January 1, 1995.

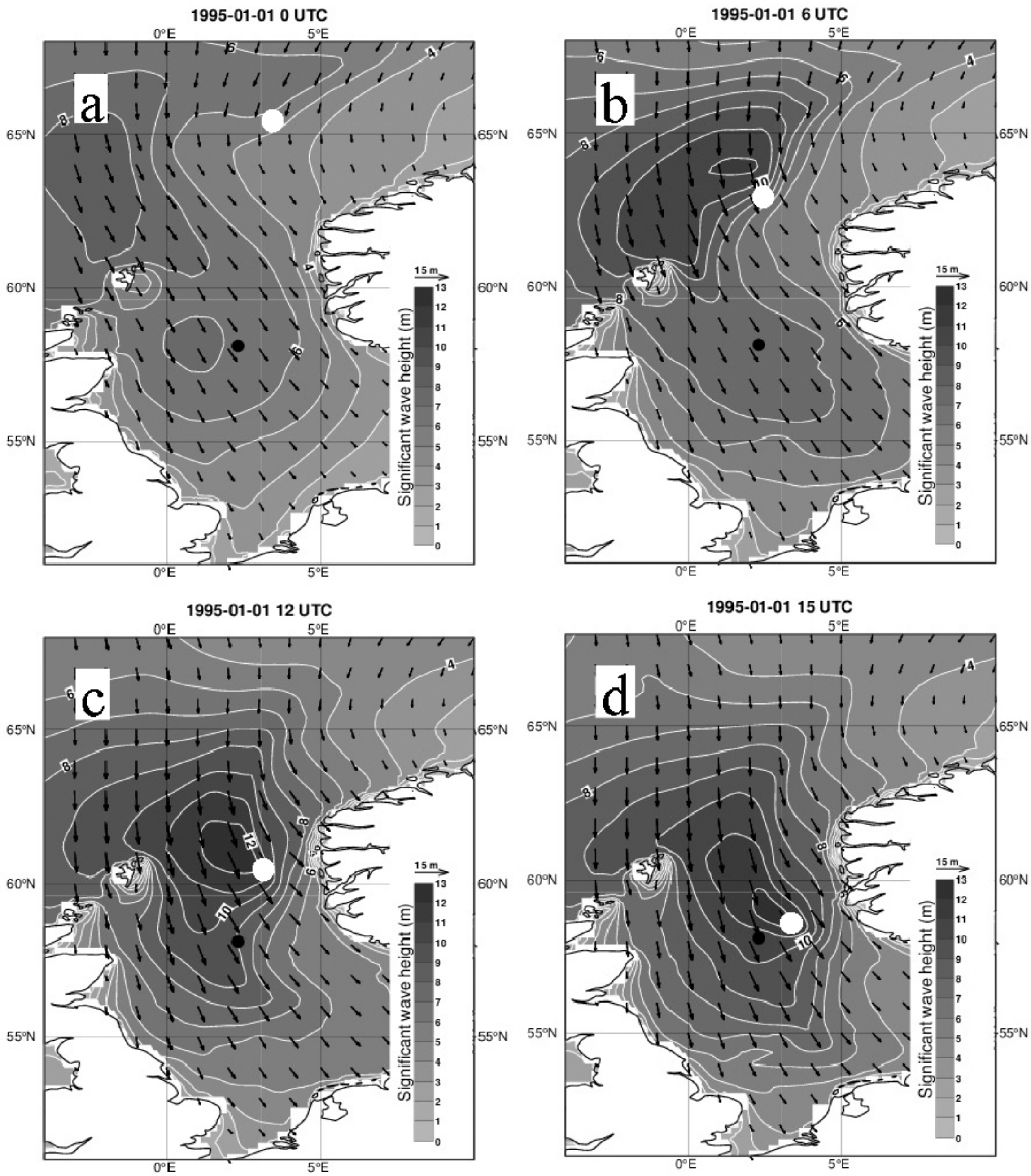

Figure 4 – Significant wave height (m) distribution in the North and Norwegian seas on 1st of January, 1995. Isolines at 0.5 m interval. The black dot shows the position of the Draupner platform. The white circles show the positions of the spectra in panels a. of Figure 5. Panels a to d at 00, 06, 12, 15 UTC respectively. See Figure 2 for the corresponding wind and surface pressure fields.

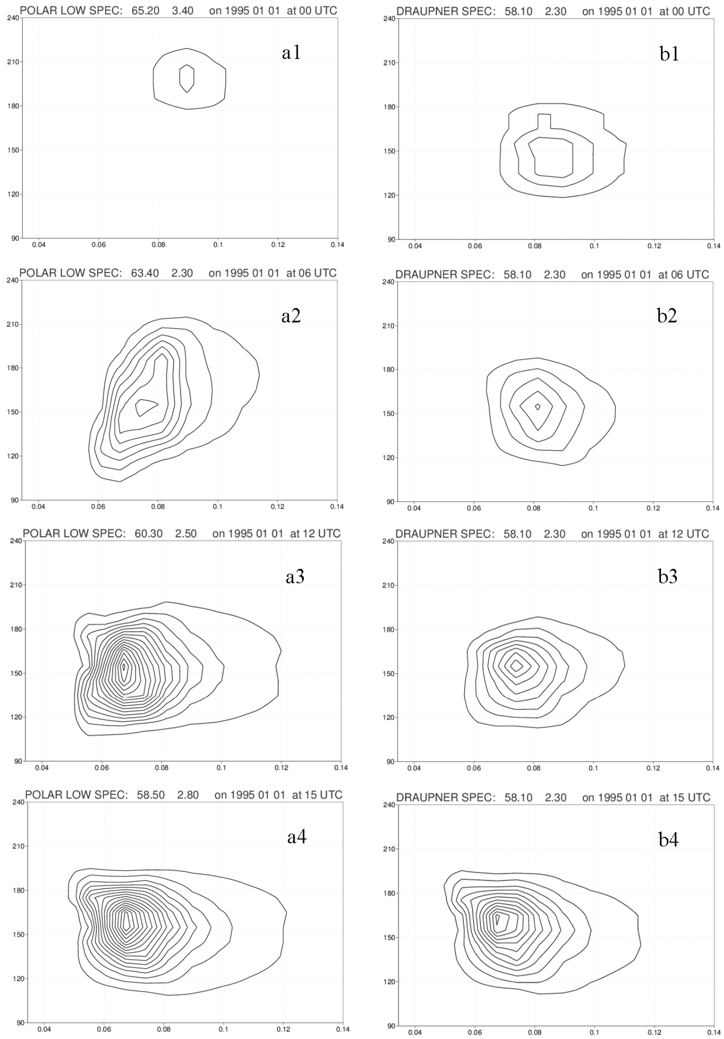

Figure 5 – Two dimensional (f-θ) wave spectra at (1 to 4) 00, 06, 12, 15 UTC respectively. Panels a. are at a position (small white circles in Figure 4) slightly to the West of the polar low (see its positions in Figure 2). Panels b. are at the Draupner position (black dot in Figure 4). Energy density isolines at 20 m^2 s rad^{-1} interval. Only the area between 0.04 and 0.14 Hz, and 90° and 140° flow directions, where energy is concentrated, is shown. Positions are as latitude North and longitude East.

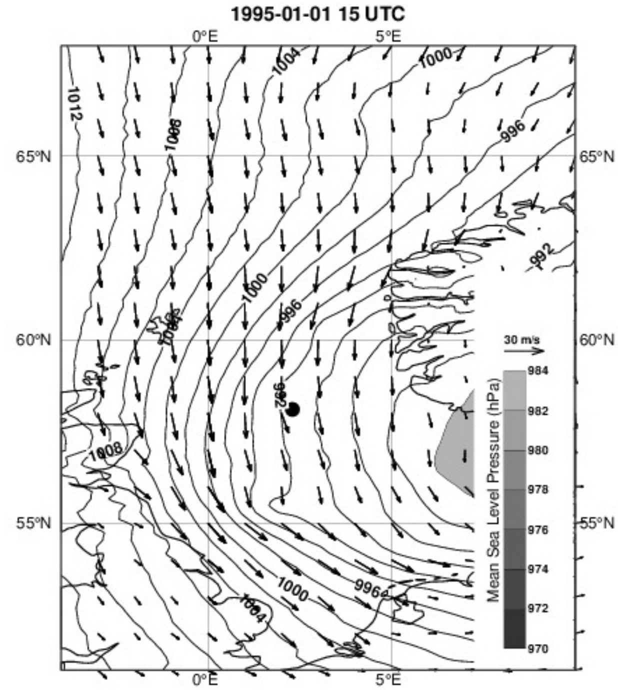

Figure 6 - Wind speed (arrows) and surface pressure (isobars) distribution in the North and Norwegian seas starting from the December 31 00 UTC analysis at +39 h forecast for 1st of January, 1995 15 UTC. Isobars at 0.5 hPa interval. The dot shows the position of the Draupner platform. Experiment gc8l (see Table 1).

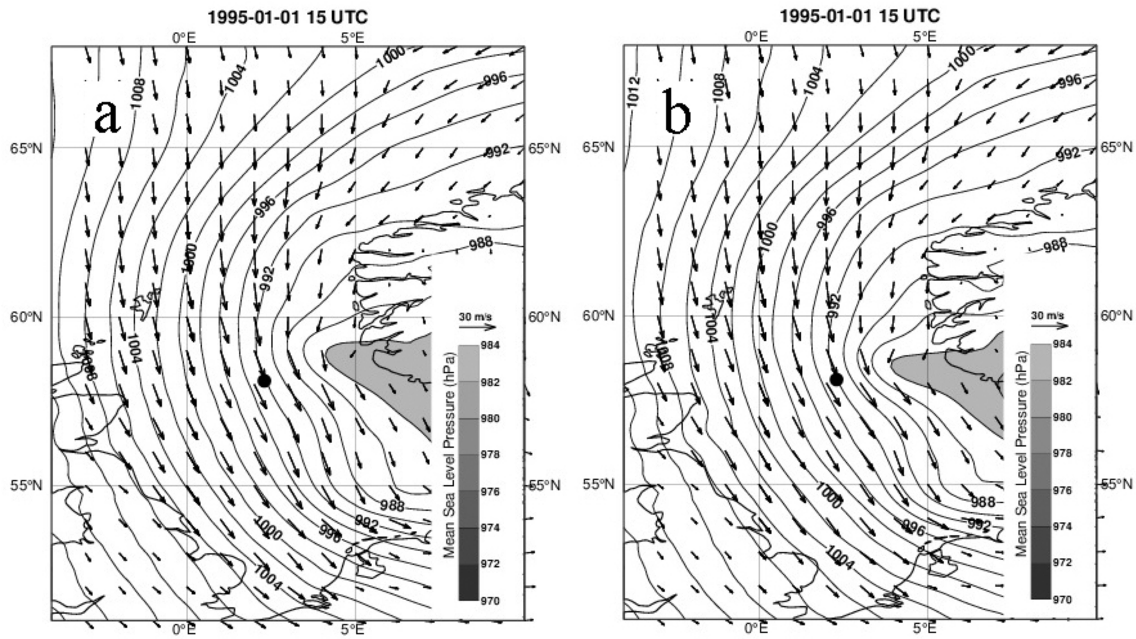

Figure 7 - Wind speed (arrows) and surface pressure (isobars) distribution in the North and Norwegian seas on 1st of January, 1995 15 UTC. 15 h forecasts from the 00 UTC analysis. Isobars at 0.5 hPa interval. The dot shows the position of the Draupner platform. Panel a according to the 1428 experiment. Panel b according to the gc9l experiment. See Table 1 for their specifications.

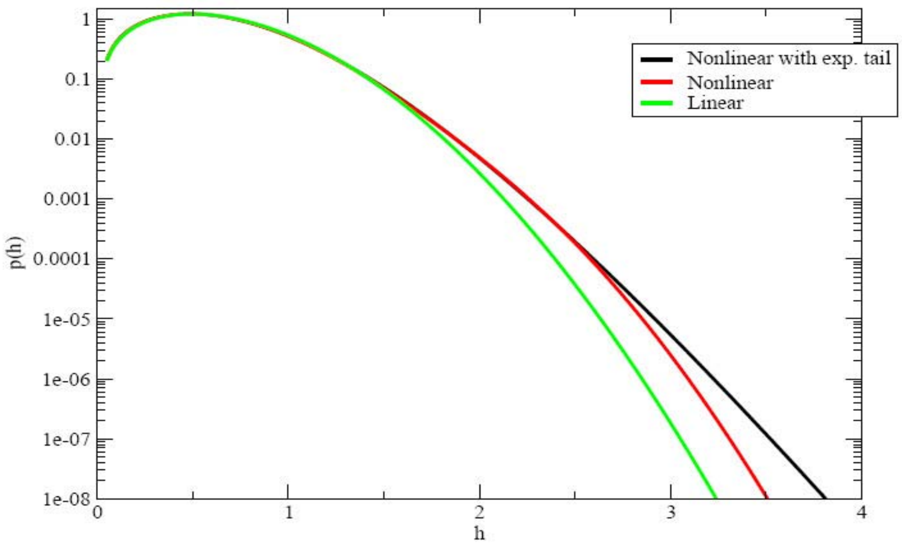

Figure 8 - Envelope wave height probability distribution function (normalized with respect to H_s) of the Draupner wave in an area 14x14 km^2, starting from the wave conditions represented by the spectra in panels a4 and b4 of Figure 5. Linear, nonlinear, and nonlinear with exponential tail distributions are considered.